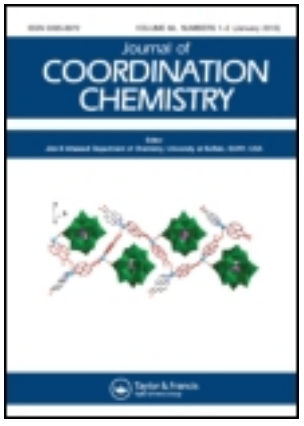

Journal of Coordination Chemistry
Publication details, including instructions for authors and subscription information:
http://www.tandfonline.com/loi/gcoo20

Two new Cu(II) m-hydroxybenzoato complexes with chloro- and carboxylato-bridged dinuclear [Cu(μ_2-Cl)(μ_2-COO)Cu] cores

Cun-Jie Lin[a], Jin-Li Qi[a], Yue-Qing Zheng[a] & Jian-Li Lin[a]
[a] Center of Applied Solid State Chemistry Research, Ningbo University, Ningbo, P.R. China
Accepted author version posted online: 10 Oct 2013.Published online: 15 Nov 2013.

To cite this article: Cun-Jie Lin, Jin-Li Qi, Yue-Qing Zheng & Jian-Li Lin (2013) Two new Cu(II) m-hydroxybenzoato complexes with chloro- and carboxylato-bridged dinuclear [Cu(μ_2-Cl)(μ_2-COO)Cu] cores, Journal of Coordination Chemistry, 66:21, 3877-3890, DOI: 10.1080/00958972.2013.853053

To link to this article: http://dx.doi.org/10.1080/00958972.2013.853053

Journal of Coordination Chemistry, 2013
Vol. 66, No. 21, 3877–3890, http://dx.doi.org/10.1080/00958972.2013.853053

Two new Cu(II) *m*-hydroxybenzoato complexes with chloro- and carboxylato-bridged dinuclear [Cu(μ_2−Cl)(μ_2−COO)Cu] cores

CUN-JIE LIN, JIN-LI QI, YUE-QING ZHENG* and JIAN-LI LIN

Center of Applied Solid State Chemistry Research, Ningbo University, Ningbo, P.R. China

(*Received 22 March 2013; accepted 21 August 2013*)

In aqueous methanolic solution, reactions of $CuCl_2$, *m*-hydroxybenzoic acid (HL), and NaOH with 2,2'-bipyridine (bpy) and 1,10-phenanthroline (phen) at room temperature afforded {[Cu(bpy)L](μ_2−Cl)(μ_2−L)[Cu(bpy)L]}·1.2H_2O (**1**) and {[Cu(phen)Cl](μ_2−Cl)(μ_2−L)[Cu(phen)L]} (**2**) with chloro- and carboxylato-bridged dinuclear [Cu(μ_2−Cl)(μ_2−COO)Cu] cores. The Cu_2 dimers in **1** are pairwise aggregated to form H-bonded tetranuclear motifs, which are extended by H_2O into 1-D H-bonded chains and further assembled into 2-D supramolecular networks. The Cu_2 dimers in **2** are also linked into 1-D H-bonded chains and further assembled into 2-D supramolecular layers. Magnetic measurements indicate that significant antiferromagnetic interactions (J = −15.9, −12.2 cm^{-1}) between Cu^{2+} ions are dominant in these dinuclear [Cu(μ_2−Cl)(μ_2−COO)Cu] cores. To the best of our knowledge, **2**, crystallizing in the acentric polar orthorhombic space group $Pna2_1$, represents the first example of metal *m*-hydroxybenzoato complexes with ferroelectric properties with a remnant polarization (*Pr*) of ca. 0.04 μC cm^{-2}, coercive field (*Ec*) of ca. 2.52 kV cm^{-1}, and saturation of the spontaneous polarization (*Ps*) at ca. 0.195 μC cm^{-2}.

Keywords: Cu(II) Complexes; Dinuclear [Cu(μ_2−Cl)(μ_2−COO)Cu] core; *m*-Hydroxybenzoic acid complexes; Magnetism; ferroelectricity

1. Introduction

Metal cluster compounds have heavy structure and potential applications in catalysis, host–guest chemistry, magnetic materials, and gas storage and separation [1–4]. Among these compounds, copper clusters are of special interest due to their structures, magnetic properties, and biological activities [5–7]. Dinuclear copper(II) cores are the simplest, and the coppers can be linked by single, double, triple, or quadruple bridges with mono-, di-, tri-, or poly-atomic bridging ligands [8–10]. The most widely investigated dinuclear copper(II) clusters are the dihydroxo-bridged [$Cu_2(OH)_2$] units and the tetracarboxylato-bridged paddle wheel-like [$Cu_2(COO)_4$] units. However, dicopper clusters containing both chloro- and carboxylato-bridges have not been explored. In the *o*-, *m*-, and *p*-hydroxybenzoic acid family, the *m*-isomer is less used as a ligand, but exhibits a variety of coordination modes (scheme 1) in the limited complexes known [11–15]. A search of the Cambridge Structural Database (CSD) revealed 33 complexes

*Corresponding author. Email: zhengcm@nbu.edu.cn

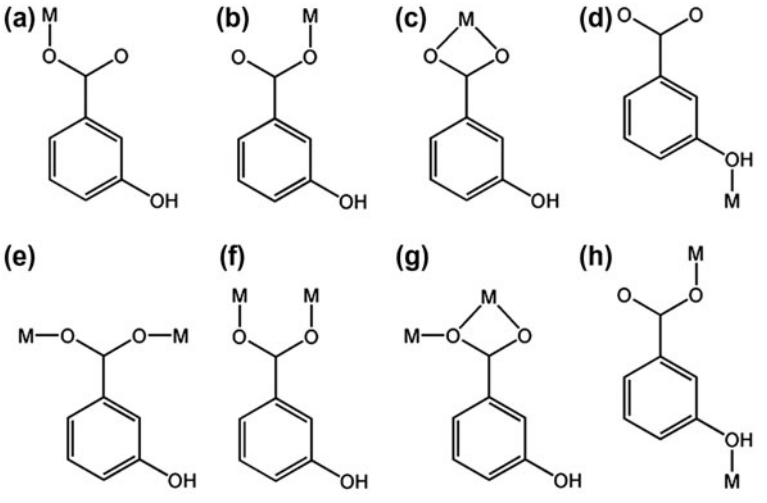

Scheme 1.

with *m*-hydroxybenzoic acid ligands; 11 of these (33%) contain dinuclear units, but no dinuclear Cu(II) complexes with both chloro- and carboxylato-bridges have been reported. Additionally, acentric crystalline materials have received much attention for their wide applications in ferroelectricity [16], pyroelectricity [17], piezoelectricity [18], triboluminescence [19], asymmetric catalysis, [20] and non-linear optical activity [21]; and design and synthesis of acentric complexes are two of the most challenging tasks in supramolecular chemistry and crystal engineering [22]. Self-assembly of $CuCl_2$, *m*-hydroxybenzoic acid (HL), and 2,2'-bipyridine (bpy) or phenanthroline (phen) in aqueous methanolic solution afforded two new chloro- and carboxylato-bridged copper(II) complexes, $\{[Cu(bpy)L](\mu_2{-}Cl)(\mu_2{-}L)[Cu(bpy)L]\}\cdot 1.2H_2O$ (**1**) and $\{[Cu(phen)Cl](\mu_2{-}Cl)(\mu_2{-}L)[Cu(phen)L]\}$ (**2**); **2** crystallizes in a polar, acentric space group and exhibits significant ferroelectric properties. Herein, we report the synthesis, structures, and magnetic properties of **1** and **2** along with the ferroelectric properties of **2**. To the best of our knowledge, **2** represents the first example of a *m*-hydroxybenzoato complex with ferroelectric properties.

2. Experimental

2.1. *Materials and physical methods*

2.1.1. Materials. All the chemicals were of reagent grade, commercially available, and used without purification.

2.1.2. Physical methods. Powder X-ray diffraction measurements were carried out with a Bruker D8 Focus X-ray diffractometer using $CuK_{\alpha 1}$ radiation of wavelength 1.54012 Å at a scan speed of $10^\circ\ s^{-1}$ to check phase purity. Single crystal X-ray diffraction data were collected on a Rigaku R-axis–Rapid X-ray diffractometer. C, H, and N microanalyses were performed with a Perkin Elmer 2400II elemental analyzer. FT–IR spectra were recorded

from KBr pellets in the range 4000–400 cm^{-1} on a Shimadzu FTIR–8900 spectrometer. Thermogravimetric measurements were carried out from room temperature to 800 °C on preweighed samples under nitrogen using a Seiko Exstar 6000 TG/DTA 6300 apparatus with a heating rate of 10 °C min^{-1}. The temperature-dependent magnetic susceptibilities were determined with a Quantum Design SQUID magnetometer (Quantum Design model MPMS-7) from 2 to 300 K with an applied field of 1 KOe and diamagnetic corrections estimated from Pascal's constants [23] ($\chi_{dia} = -470.8 \times 10^{-6}$ cm^3 M^{-1} for **1** and -484.2×10^{-6} cm^3 M^{-1} for **2**). The ferroelectric properties of a solid sample of **2** were measured on a pelletized powdered sample using a Premier II ferroelectric tester at room temperature while the sample was immersed in insulating oil.

2.2. *Synthesis of {[Cu(bpy)L](μ_2−Cl)(μ_2−L)[Cu(bpy)L]}·1.2H_2O (1)*

In a typical synthetic procedure, 171.0 mg (1.00 mM) $CuCl_2 \cdot 2H_2O$, 138.0 mg (1.00 mM) *m*-hydroxybenzoic acid, 156.0 mg (1.00 mM) 2,2'-bipyridine, and 20.0 mg (0.5 mM) NaOH were separately dissolved in a mixed solvent of 5.0 mL H_2O and 5.0 mL CH_3OH. After dropwise addition of the organic acid solution to the Cu(II) solution, the bpy solution was added, during which the incipiently formed bluish flocculent precipitate dissolved rapidly on stirring to give a light blue solution. Subsequently, the NaOH solution was added dropwise, affording a dark blue solution (pH = 3.84), which was then allowed to stand at room temperature for slow evaporation. About 10 days later, well-shaped blue crystals (0.098 g, 32.4% yield) appeared in solution and were isolated. Anal. Calcd for $C_{41}H_{33.4}ClCu_2N_4O_{10.2}$ (%): C, 54.24; H, 3.71; N, 6.17. Found: C, 54.28; H, 3.78; N, 6.22. IR data (cm^{-1}, KBr): 3479m(br), 3373m(mult), 3140s(br), 2928w(mult), 1602s(sh), 1560vs(shp), 1474s(shp), 1447vs(shp), 1418m(sh), 1377vs(shp), 1252s(shp), 1225s(sh), 1159m(shp), 1107w(shp), 1034w(shp), 933w(shp), 895w(shp), 802w(shp), 766vs(shp), 731s(shp), 692w(shp) (where br = broad, mult = multiplet, shp = sharp, sh = shoulder).

2.3. *Synthesis of {[Cu(phen)Cl](μ_2−Cl)(μ_2−L)[Cu(phen)L]} (2)*

Complex **2** was synthesized analogous to **1** except that 198.0 mg (1.0 mM) phenanthroline monohydrate was used instead of bpy. Slow evaporation of the resulting dark blue solution (pH = 2.46) over five days afforded well-shaped blue crystals (0.196 g, 47.1% yield). Anal. Calcd for $C_{38}H_{26}Cl_2Cu_2N_4O_6$ (%): C, 54.82; H, 3.15; N, 6.73. Found: C, 54.86; H, 3.18; N, 6.79. IR data (cm^{-1}, KBr): 3419m(br), 3184vw(mult), 3090vw(mult), 2925vw(mult), 1603w(sh), 1545vs(shp), 1518m(shp), 1447m(shp), 1425m(shp), 1396vs (shp), 1342s(shp), 1256m(mult), 1223m(mult), 1145m(mult), 1107s(shp), 997w(mult), 937w(mult), 847vs(shp), 771vs(shp), 721vs(shp) (where br = broad, mult = multiplet, shp = sharp, sh = shoulder).

2.4. *X–ray crystallography*

Suitable single crystals were selected under a polarizing microscope and fixed with epoxy cement on fine glass fibers which were then mounted on a Rigaku R-Axis–Rapid

diffractometer with graphite-monochromated Mo K_α radiation ($\lambda = 0.71073$ Å) for cell determination and subsequent data collection. The reflection intensities in suitable θ ranges were collected at 293 K using the ω scan technique. The single crystals exhibit no detectable decay during the data collection. The data were corrected for *Lp* and absorption

Table 1. Crystal data, data collection, structure solution and refinement parameters for **1** and **2**.

Parameter	**1**	**2**
Empirical formula	$C_{41}H_{33.40}ClCu_2N_4O_{10.20}$	$C_{38}H_{26}Cl_2Cu_2N_4O_6$
Formula mass	907.87	832.63
Crystal system	Triclinic	Orthorhombic
Space group	$P\bar{1}$	$Pna2_1$
a (Å)	10.4862(5)	13.504(3)
b (Å)	11.5582(6)	18.167(4)
c (Å)	17.0841(9)	13.545(3)
α (°)	78.6773(17)	90
β (°)	72.9206(14)	90
γ (°)	82.5906(14)	90
Volume (Å^3)	1934.86(17)	3323.0(13)
Z	2	4
D_{Calcd} (g·cm^{-3})	1.558	1.664
$F(000)$	928	1688
μ (mm^{-1})	1.234	1.498
Total No. of data collected	18,999	29,583
No. of obsd. data ($I \geq 2\sigma(I)$)	5677	3980
θ Range (°)	3.20–27.47	3.01–27.470
Goodness–of–fit on F^2	1.040	0.995
R_1, wR_2 [$I \geq 2\sigma(I)$][a]	0.0521, 0.1383	0.0732, 0.1518
R_1, wR_2 (all data)[a]	0.0874, 0.1776	0.1416, 0.1807
Flack x parameter	–	0.00
No. of variables	532	472
$\delta\rho_{max}$, $\delta\rho_{min}$e.Å^{-3}	0.686, −1.315	1.145, −0.491

[a]$R_1 = \sum(|F_o|-|F_c|)/\sum|F_o|$, $wR_2 = [\sum w(F_o^2-F_c^2)^2/\Sigma w(F_o^2)^2]^{1/2}$, and $w = [\sigma^2(F_o^2)+(aP)^2 + bP]^{-1}$, where $P = (F_o^2 + 2F_c^2)/3$. For **1**, $a = 0.0975$ and $b = 0.0000$. For **2**, $a = 0.0844$ and $b = 0.0000$.

Table 2. Selected bond distances (Å) and angles (°) and hydrogen bonding parameters for **1**.[a]

Cu1–O4	1.940(3)	Cu1–O1	1.963(3)	Cu1–N2	2.000(3)
Cu1–N1	2.026(3)	Cu1–Cl	2.556(1)	Cu2–O7	1.928(3)
Cu2–O2	1.961(3)	Cu2–N4	1.988(3)	Cu2–N3	2.020(3)
Cu2–Cl	2.593(1)				
O1–Cu1–O4	94.58(12)	N2–Cu1–O4	173.12(12)	N2–Cu1–O1	89.40(12)
N1–Cu1–O4	94.01(12)	N1–Cu1–O1	153.33(12)	N1–Cu1–N2	80.02(12)
Cl–Cu1–O4	95.14(9)	O1–Cu1–Cl	102.34(8)	Cl–Cu1–N2	89.47(10)
Cl–Cu1–N1	101.96(10)	O2–Cu2–O7	91.05(12)	N4–Cu2–O7	167.64(12)
Cl–Cu2–O7	101.46(9)	N3–Cu2–O7	91.99(12)	N4–Cu2–O2	92.77(12)
N3–Cu2–O2	159.95(13)	Cl–Cu2–O2	99.27(9)	N3–Cu2–N4	80.49(13)
Cl–Cu2–N4	89.52(10)	Cl–Cu2–N3	99.53(10)		
Hydrogen bonding contacts					
D–H···A	D–H	H···A	D···A	D–H···A	
O3–H3B···O10	0.820	1.920	2.734	171.23	
O6–H6B···O8$^{\#1}$	0.820	1.947	2.755	167.93	
O9–H91···Cl$^{\#2}$	0.920	2.114	3.033	178.32	
O10–H101···O9$^{\#3}$	0.872	1.964	2.835	176.12	
O10–H102···O5	0.871	1.944	2.814	177.87	
O11–H111···O4$^{\#2}$	0.851	2.266	3.117	178.43	
O11–H112···O8	0.861	2.021	2.881	178.27	

[a]Symmetry transformations used to generate equivalent atoms: #1 = $-x + 1, -y + 2, -z + 1$; #2 = $x + 1, y, z$; #3 = $x - 1, y + 1, z$.

Table 3. Selected bond distances (Å) and angles (°) and hydrogen bonding parameters for **2**[a].

Cu1–O1	1.962(4)	Cu1–N1	2.009(5)	Cu1–N2	2.019(4)
Cu1–Cl1	2.282(2)	Cu1–Cl2	2.517(2)	Cu2–O2	1.945(4)
Cu2–O4	1.975(4)	Cu2–N4	2.000(4)	Cu2–N3	2.034(4)
Cu2–Cl1	2.621(2)	Cu2–O5	2.734(4)		
O1–Cu1–N1	91.97(6)	O1–Cu1–N2	161.36(7)	O1–Cu1–Cl1	91.23(2)
O1–Cu1–Cl2	100.20(1)	N1–Cu1–N2	80.55(7)	N1–Cu1–Cl1	162.16(3)
N1–Cu1–Cl2	91.23(3)	N2–Cu1–Cl1	91.99(4)	N2–Cu1–Cl2	96.58(3)
Cl1–Cu1–Cl2	105.79(6)	O2–Cu2–O4	91.31(6)	O2–Cu2–N4	172.23(8)
O2–Cu2–N3	93.40(7)	O2–Cu2–Cl1	87.36(2)	O4–Cu2–N4	96.26(8)
O4–Cu2–N3	149.71(8)	O4–Cu2–Cl1	92.41(2)	N4–Cu2–N3	80.94(8)
N4–Cu2–Cl1	90.56(2)	N3–Cu2–Cl1	117.78(4)	O4–Cu2–O5	53.96(4)
N3–Cu2–O5	95.94	N4–Cu2–O5	80.61	O5–Cu2–O2	105.19
Cl1–Cu2–O5	143.31				
Hydrogen bonding contacts					
D–H···A	D–H	H···A	D···A	D–H···A	
O6–H61···Cl2$^{\#1}$	0.932	2.104	3.035	179.11	
O3A–H3AA_a···O5$^{\#2}$	0.820	1.910	2.712	165.60	
O3B–H3BA_b···O5$^{\#2}$	0.820	1.930	2.718	160.92	

[a]Symmetry transformations used to generate equivalent atoms: #1 = *x*, *y*, *z* + 1; #2 = −*x* + 3/2, *y* + 1/2, *z*−1/2.

effects. The structure was solved by direct methods employing SHELXS-97 [24] and was refined by subsequent difference Fourier synthesis also using SHELXL-97 [25]. Structural refinements showed that one lattice water molecule in **1** was disordered with partial occupancy of ca. 20% (O11), and one hydroxyl oxygen atom (O3) of L^- in **2** was split over two positions with 50 : 50 occupancies. The hydrogen atoms attached to carbon were geometrically generated, while the remaining hydrogen atoms were located from successive difference Fourier syntheses. The full-matrix least-squares technique was applied for refinement of positions and anisotropic displacement parameters of all the non-hydrogen atoms, and positions of hydrogen atoms were refined using a riding mode by fixing the initial distances to the associated heavier atoms with the isotropic displacement parameters set to 1.2 times the values for the associated atoms. Crystal data and structure and refinement parameters are summarized in table 1. Selected bond distances and angles are given in tables 2 and 3.

3. Results and discussion

3.1. *Syntheses*

In an aqueous methanolic solution, $CuCl_2{\cdot}2H_2O$, HL, bpy, and NaOH reacted to yield {[Cu(bpy)L](μ$_2$−Cl)(μ$_2$−L)[Cu(bpy)L]}·1.2H_2O (**1**); substitution of phen for the bpy resulted in an anhydrous product {[Cu(phen)Cl](μ$_2$−Cl)(μ$_2$−L)[Cu(phen)L]} (**2**). The reactions are as follows:

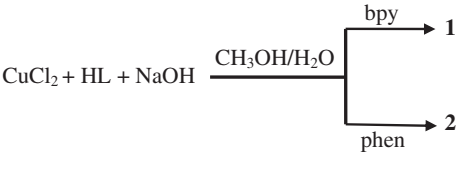

Upon exposure to air, crystals of **1** and **2** retain their crystallinity and luster for a longer time, suggesting them to be air-stable. Product purities were checked by PXRD, and the experimental and simulated PXRD patterns are shown in the Supplementary material. The peak positions in the experimental and simulated patterns are in agreement, indicating good phase purity. The differences in intensity may be due to preferred orientations of the powdered samples.

3.2. *Description of the crystal structures*

3.2.1. {[Cu(bpy)L](μ_2−Cl)(μ_2−L)[Cu(bpy)L]}·1.2H_2O (1). Compound **1** crystallizes in the triclinic space group $P\bar{1}$ and the structure is shown in figure 1. Of the three crystallographically distinct L^-, two are monodentate (scheme 1(a,b)), while the third is a μ_2-κO : κO' bridging ligand with the carboxylate in a syn–syn mode (scheme 1(f)) [26]. The carboxylate of the latter L^- is severely twisted, with a 27.5(5)° dihedral angle between the carboxylate group and the benzene ring, while both terminal L^- show less twisting with corresponding angles of 6.8(6) and 14.2(5)°. The Cl^- serves as a μ_2-bridge between Cu(1) and Cu(2). The Cl^- bridge is slightly asymmetric, with Cu(1)–Cl and Cu(2)–Cl bond distances of 2.556(1) and 2.593(1) Å, respectively (table 2). The chelating bpy ligands exhibits nearly perfect coplanarity. The Cu ions are each in a square pyramidal $CuClN_2O_2$ chromophore defined by an apical Cl^-, a bpy molecule, and two L^-. The equatorial Cu−N/O distances vary from 1.928 to 2.026 Å. The *cis* and *trans* angles around Cu are 80.0−102.3°

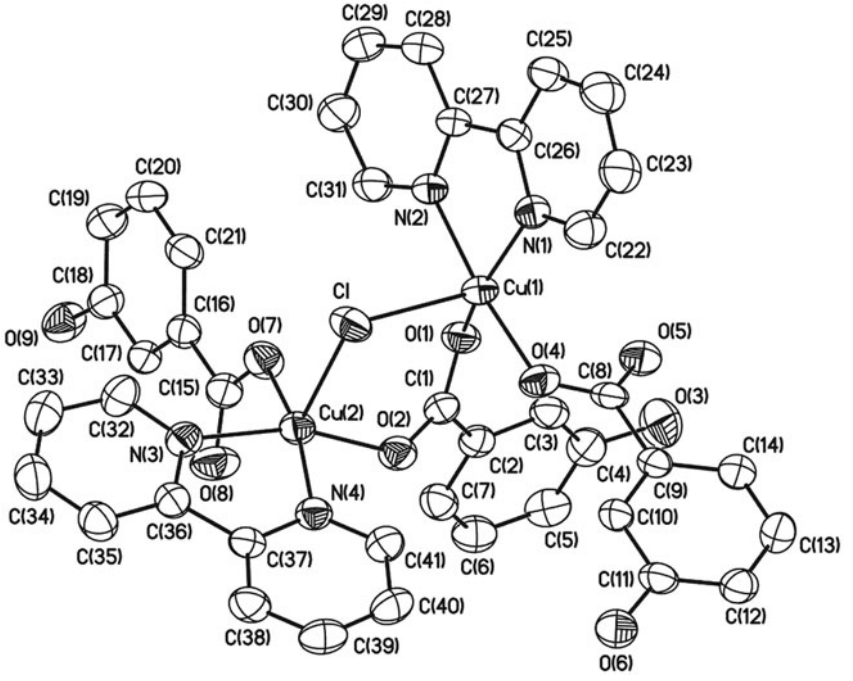

Figure 1. ORTEP view of [Cu(bpy)L](μ_2−Cl)(μ_2−L)[Cu(bpy)L], **1**, with 45% probability displacement ellipsoids. Crystalline water is not shown.

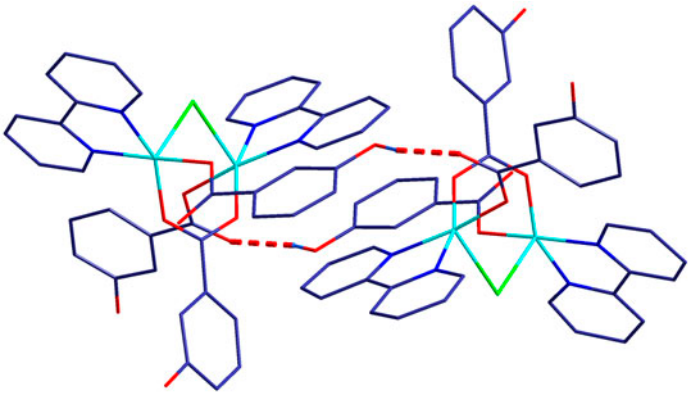

Figure 2. H-bonded tetranuclear motifs assembled from a pair of adjacent dinuclear molecules in **1**.

and 153.3−173.1°, respectively. Cu(1) and Cu(2) exhibit τ values of 0.33 and 0.128 [27], each shifted towards the Cl apex from the N_2O_2 base by 0.253(2) and 0.261(2) Å, respectively. All these values suggest the square pyramidal ClN_2O_2 coordination geometry to be significantly distorted. The μ_2−Cl^- and μ_2-κO : κO' L^- anions bridge two $[Cu(bpy)L]^+$ moieties to generate dinuclear {[Cu(bpy)L](μ_2−Cl)(μ_2−L)[Cu(bpy)L]}. The O_6 hydroxyl of the monodentate L^- coordinated to Cu(1) donates its H to the uncoordinated carboxylate O_8 of another monodentate L^- coordinated to Cu(2) of a neighboring molecule to form a nearly linear hydrogen bond with $d(O_6{-}H{\cdots}O_8^{\#1}) = 2.755$ Å and $\angle(O_6{-}H{\cdots}O_8^{\#1}) = 168°$ (#1 = −x + 1, −y + 2, −z + 1). Through these intermolecular hydrogen bonds, the adjacent molecules are paired to generate hydrogen-bonded centrosymmetric tetranuclear motifs (figure 2). Owing to hydrogen-bonding interactions, the tetranuclear motifs are held together by lattice waters to build 1-D chains extending in the [1$\bar{1}$0] direction, and the formed chains are assembled via O−H···Cl hydrogen bonds into 2-D supramolecular networks parallel to (001) as shown in figure 3. Along the crystallographic *a*-axis, the 2-D networks are stacked in an ···AAA··· sequence [28], and the disordered lattice waters are located between the networks.

3.2.2. {[Cu(phen)Cl](μ_2−Cl)(μ_2−L)[Cu(phen)L]} (2). Complex **2** crystallizes in the polar acentric orthorhombic space group *Pna*2_1 (No. 33) with the point group *mm2*. The structure is shown in figure 4. The crystallographically independent L^- are either an asymmetrically chelating ligand (scheme 1(c)) or a bidentate μ_2-κO : κO' ligand, bridging Cu(1) and Cu(2) with carboxylate in a syn–syn coordination (scheme 1(f)) [26]. The Cl^- anions are monodentate and bridging. The bridging Cu(1)–Cl(1) and Cu(2)–Cl(1) bond distances are 2.282(2) and 2.621(2) Å, respectively, and the Cu(1)–Cl(2) bond distance is 2.517(2) Å. The Cu–O and Cu–N bond distances are 1.945–1.975 and 2.000–2.034 Å, except for the long Cu(2)–O(5) bond distance of 2.734(4) Å of the asymmetrically chelating L^-. The carboxylates of the chelating and bidentate L^- are less twisted in comparison with **1**, with dihedral angles between the carboxylate and phenyl rings of 9.8(5)° and 5.5(5)°, respectively. Cu(1) exhibits a square-pyramidal $CuCl_2N_2O$ chromophore with Cl(2) at the apex. The τ value of 0.38 [27] together with

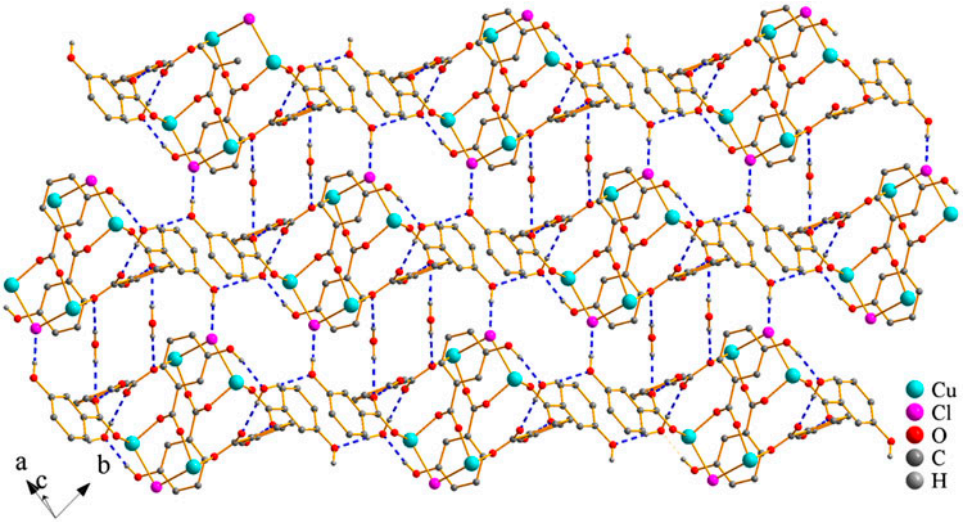

Figure 3. 2-D supramolecular network in **1**.

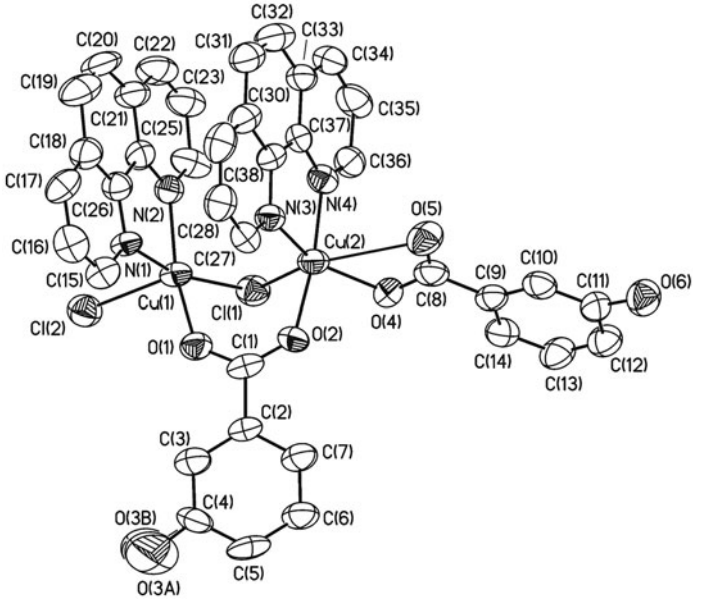

Figure 4. ORTEP view of [Cu(phen)Cl](μ_2−Cl)(μ_2−L)[Cu(phen)L], **2**, with 45% probability displacement ellipsoids.

the bonding parameters (table 3) indicate the Cl_2N_2O polyhedron to be significantly distorted with copper shifted by 0.233(4) Å from the basal plane towards the apex. Cu (2) has an elongated octahedral $CuClN_2O_3$ chromophore of "4 + 2" coordination type

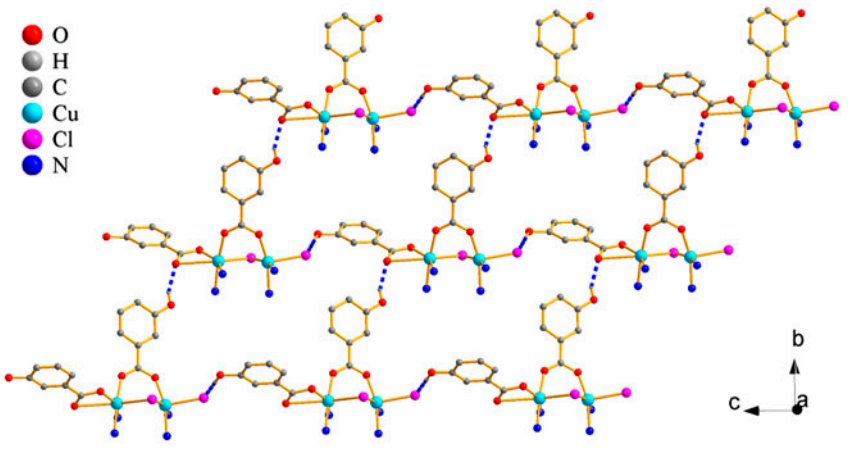

Figure 5. 2-D supramolecular network in **2**.

due to the Jahn–Teller effect [29]. Both $[Cu(phen)Cl]^+$ and $[Cu(phen)L]^+$ are co-bridged by Cl^- and L^- to give dinuclear {[Cu(phen)Cl](μ$_2$−Cl)(μ$_2$−L)[Cu(phen)L]}. The phen ligands are nearly parallel, with a dihedral angle of 4.58(5)°, and the mean interplanar distance of 3.40 Å suggests substantial intermolecular $\pi\cdots\pi$ stacking interactions between phen ligands. The bridging Cl(1) occupies equatorial and apical sites of Cu(1) and Cu (2), different from **1**, where the bridging Cl(1) is situated at the apical sites of both the metals. The O3 hydroxyl of the bridging L^- forms an intermolecular O−H···O hydrogen bond to the weakly bound carboxylate $O5^{\#1}$ of a second L^- in the complex's neighbor (#1 = $-x + 3/2$, $y + 1/2$, $z - 1/2$), leading to 1-D chains extending in the [011] direction. The O6 hydroxyl of the terminal L^- donates its H to the terminal $Cl(2)^{\#2}$ (#2 = x, y, $z + 1$) to form intermolecular O−H···Cl hydrogen bonds, which expand the 1-D chains to 2-D supramolecular layers parallel to (100) (figure 5); along the crystallographic *a*-axis the resulting 2-D layers are stacked in an ···ABABAB··· sequence [28].

Comparison of **1** and **2** shows that the Cu(1)···Cu(2) separation of 3.854 Å in **1** is larger than the value of 3.195 Å in **2**, and the bridging angles Cu(1)–Cl(1)–Cu(2) in these two compounds are 96.92(4)° and 81.00(8)°, respectively. While chloro- and carboxylate-bridged dicopper clusters are unknown in literature, a few triply-bridged dimeric complexes which contain a chloro- and a carboxylate-bridge have been reported. The Cu–Cl–Cu bond angles in these complexes are between 70.16(2)° and 89.98(5)°. The Cu–Cl bond distances and the Cu···Cu separation in these complexes fall in the ranges 2.326(3)–2.884(4) and 2.957(3)–3.564(2) Å, respectively [30–32].

3.3. *Infrared spectra*

IR spectra of **1** and **2** (Supplementary material) show features attributable to each component of the complexes and are compatible with the structures. For **1**, absorptions at 3700−3000 cm^{-1} are due to O−H stretches of lattice waters and OH of L^-. Sharp, strong

peaks at 1602 and 1560 cm^{-1} are attributable to the asymmetric $-CO_2$ vibrations ($\nu_{as}(CO_2^-)$) of carboxylate of L^-, and peaks at 1418 and 1377 cm^{-1} to the symmetric $-CO_2$ vibrations ($\nu_s(CO_2^-)$). Based on the spectra of bpy and HL, the absorption peaks at 1474 and 1447 cm^{-1} are assigned to the C=N and C=C vibrations of the pyridyl ring, and the ν_{Ar-O} stretches generate two absorptions at 1252 and 1225 cm^{-1}. The ν_{C-H} results in a weak absorption at 2928 cm^{-1}, and the out-of-plane C−H vibrations lead to absorptions at 850−650 cm^{-1}. Absorptions due to Cu−O and Cu−Cl vibrations appear below 550 cm^{-1}. The IR spectrum of **2** exhibits absorptions in the area 3500−3000 cm^{-1} with three maxima around 3419, 3184, and 3090 cm^{-1}, belonging to O–H vibrations of the L^- anions. The absorptions due to the asymmetric $-CO_2$ stretching vibrations ($\nu_{as}(CO_2^-)$) of the carboxylate groups of the L^- anions are observed at 1603 and 1545 cm^{-1}, and peaks at 1425, 1339, and 1342 cm^{-1} originate from the symmetric $-CO_2$ stretching vibrations [33].

3.4. *Thermal analysis*

Both **1** and **2** are air-stable at room temperature; however, decomposition occurs at an elevated temperature. Thermal analysis (Supplementary material) shows **1** to be stable below 110 °C, and the weight loss of 2.64 wt.% at 190 °C is in agreement with the value of 2.38 wt.% calculated for 1.2 M H_2O per formula, implying complete dehydration. Upon further heating, the dehydrated intermediate loses weight rapidly, followed by a gradual weight loss from ca. 285 °C onwards, and ultimately gives a black solid of 21.85 wt.% at 800 °C, which corresponds well to the value of 21.87% for 1 M of Cu, 1 M of CuCl, and 3 M of C. Thermogravimetric analysis of **2** shows that it is thermally stable up to ~235 °C and upon further heating it starts decomposition in three successive steps, namely, two abrupt weight losses plus a gradual one, consistent with the decomposition of phenanthroline followed by the deconstruction of the remaining material. The final black solid at 800 °C is consistent with a mixture of 2 M of CuCl and 6 M of C (observed, 31.84 wt.% and calculated, 32.44 wt.%).

3.5. *Magnetic properties*

Temperature-dependent magnetic susceptibility measurements for **1** and **2** were performed on polycrystalline samples at 2–300 K in a fixed magnetic field of 1 KOe, and the $\chi_m T$ and χ_m (inset) *versus* T plots are shown in figure 6 (χ_m is the molar magnetic susceptibility for two Cu^{II} ions).

The magnetic behavior of **1** reveals a $\chi_m T$ value of 0.752 $cm^3\ M^{-1}\ K$ in room temperature, which is in agreement with the spin-only value of 0.750 $cm^3\ M^{-1}\ K$ expected for two isolated Cu(II) ions ($S = 1/2$ and $g = 2.0$). Upon lowering the temperature, the $\chi_m T$ value remains almost constant until ca. 90 K and then decreases abruptly to reach 6.0×10^{-3} $cm^3\ K\ M^{-1}$ at 2 K. These features are characteristic of significant antiferromagnetic coupling. The χ_m *versus* T plot displays a maximum value of 0.0156 $cm^3\ M^{-1}$ at 29 K in χ_m, which is the signature characteristic of antiferromagnetic coupling. Below 4.5 K, an increase in the χ_m values appears due to the presence of a small amount of paramagnetic impurity. The singlet–triplet energy gap (J) was deduced from the least-squares fit of the experimental data *versus* T for isotropic exchange in a copper(II) dimer, according to the Bleaney–Bowers equation modified by Kahn, taking into account some paramagnetic impurities [34], always evident when the antiferromagnetic coupling is very strong:

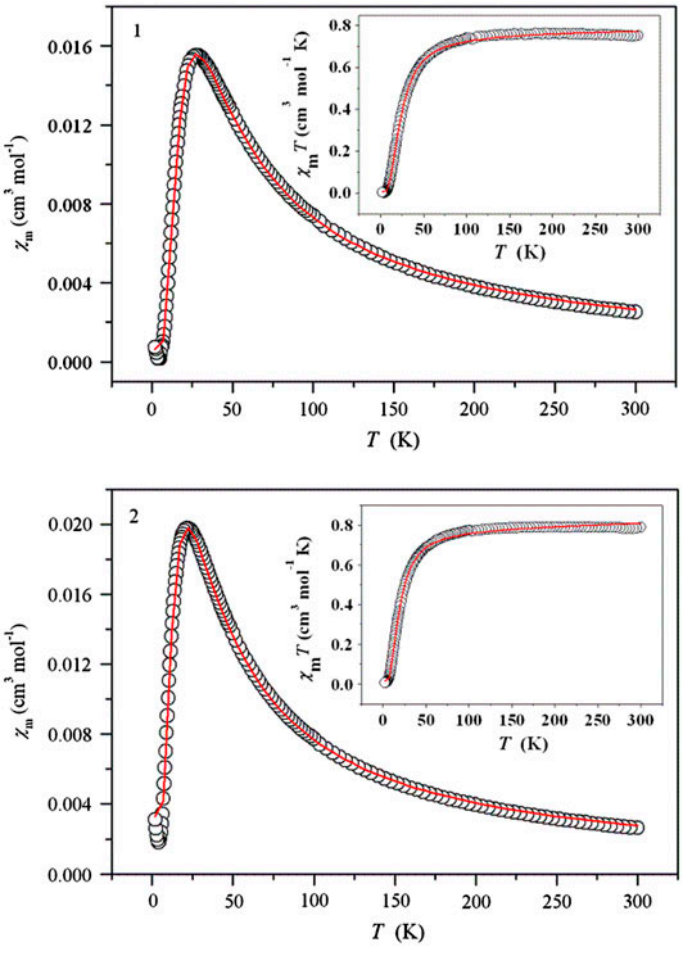

Figure 6. Temperature dependence of the magnetic susceptibilities of **1** and **2**. χ_m is the magnetic susceptibility per two Cu(II) ions.

$$\chi_{\mathrm{di}} = (1-\rho)\frac{2N\beta^2 g^2}{3kT}\left[1+\frac{1}{3}\exp(-2J/kT)\right]^{-1} + 2\rho\left(\frac{N\beta^2 g_i^2}{4kT}\right) + \mathrm{TIP} \qquad (1)$$

The Hamiltonian employed is $H = -JS_1S_2$ (where N is the Avogadro's number; g, the spectroscopic splitting factor; β, the Bohr magneton; k, the Boltzmann's constant; J, the exchange parameter; TIP, the temperature-independent paramagnetism; and ρ, the percentage noncoupled impurity). The experimental magnetic susceptibility data fit poorly to the theoretical expression in equation (1) and gave $g = 2.134(7)$, $J = -15.7(5)\,\mathrm{cm}^{-1}$, $\rho = 4.15$ (4), and TIP = 1.20×10^{-5} emu M^{-1}. The parameter ρ from this fit is abnormal, especially since the sample was confirmed to be pure phase by the experimental PXRD. So the expression in equation (1) was corrected using the molecular field approximation (equation (2)), to which the measured magnetic susceptibility data were fitted:

$$\chi_m = \frac{\chi_{di}}{1 - (2zJ/Ng^2\beta^2)\chi_{di}} \quad (2)$$

where χ_m is the exchange-coupled magnetic susceptibility actually measured, χ_{di} is the magnetic susceptibility in the absence of the exchange field, and zJ' is the total exchange parameter between dinuclear partners (z is the number of nearest neighbors). The best fit afforded values of $g = 2.019(3)$, $J = -15.9(2)\,cm^{-1}$, $zJ' = 5.4(3)\,cm^{-1}$, $\rho = 0.008(3)$, and TIP $= 120 \times 10^{-6}$ emu M^{-1}, and the agreement factor R is 7.0×10^{-5} ($R = \Sigma[(\chi_m)^{obs} - (\chi_m)^{Calcd}]^2/[(\chi_m)^{obs}]^2$). The negative J value of $-15.9(2)\,cm^{-1}$ indicates significant antiferromagnetic coupling for Cu(μ–Cl)(μ–OCO)Cu, and the small positive zJ' value of $5.4(3)\,cm^{-1}$ confirms weak ferromagnetic transmitting effects of the interdimer hydrogen bonds. The ferromagnetic exchange through H bonds is quite unusual.

Complex **2** exhibits $\chi_m T$ and χ_m (inset) *versus* T plots similar to **1**. The χ_m value is 2.63×10^{-3} cm^3 M^{-1} at room temperature, and upon lowering the temperature it monotonically increases to a maximum of 0.0198 cm^3 M^{-1} at ca. 22 K, goes through a minimum of $1.82 \times 10^{-3}\,cm^3$ M^{-1} at ca. 4 K, and then followed by an increase to 3.11×10^{-3} cm^3 M^{-1} at 2 K. The χ_m curve is typical for very strong antiferromagnetic coupling with a small amount of monomeric copper(II) impurities, manifested at a low temperature. The room temperature $\chi_m T$ value is 0.788 cm^3 M^{-1} K and agrees well with the spin-only value of 0.750 cm^3 M^{-1} K expected for two isolated Cu(II) ions ($S = 1/2$ and $g = 2.0$). Upon lowering the temperature, the $\chi_m T$ value remains almost constant until ca. 90 K, and then decreases rapidly to 6.2×10^{-3} cm^3 K M^{-1} at 2 K. The $\chi_m T$ curve is also indicative of strong antiferromagnetic coupling. Similar to **1**, the magnetic data can be analyzed, giving the best-fit results as follows: $g = 2.098(4)$, $J = -12.15(2)\,cm^{-1}$, $zJ' = 0.9(1)\,cm^{-1}$, $\rho = 0.0077$ (2), and TIP $= 120 \times 10^{-6}$ emu M^{-1}, and the agreement factor R is 1.64×10^{-8} ($R = \Sigma[(\chi_m)^{obs} - (\chi_m)^{Calcd}]^2/[(\chi_m)^{obs}]^2$). The antiferromagnetic J value for **2** is smaller than that for **1**, suggesting an unfavorable coupling interaction between two Cu atoms in **2** although the intradimer Cu···Cu separation of 3.193 Å in **2** is substantially smaller than that of 3.854 Å in **1**.

3.6. *Ferroelectric properties of two*

Acentric symmetry is a prerequisite for technologically important properties such as ferroelectricity and second-order nonlinear optical behavior [35]. As stated above, **2** crystallizes in the polar acentric space group $Pna2_1$ (No. 33) with the point group *mm2* belonging to one of the 10 polar point groups (C_1, C_s, C_2, C_{2v}, C_4, C_{4v}, C_3, C_{3v}, C_6, and C_{6v}), which are required for ferroelectricity. Therefore, **2** was subjected to test for its ferroelectric effects. Experimental measurements indicate a significant electric hysteresis loop (figure 7), which is typical of ferroelectric behavior. The remnant polarization (Pr) is ca. 0.040 μC cm^{-2} and the coercive field (Ec) is ca. 2.52 kV cm^{-1}. Saturation of the spontaneous polarization (Ps) occurs at ca. 0.195 μC cm^{-2}, which is close to that for a typical ferroelectric compound (e.g. $NaKC_4H_4O_6{\cdot}H_2O$, Rochelle's salt; usually $Ps = 0.25$ μC cm^{-2}), but significantly smaller than that observed in KDP (ca. 5 μC cm^{-2}). To the best of our knowledge, **2** represents the first example of a metal *m*-hydroxybenzoato complex with ferroelectric properties.

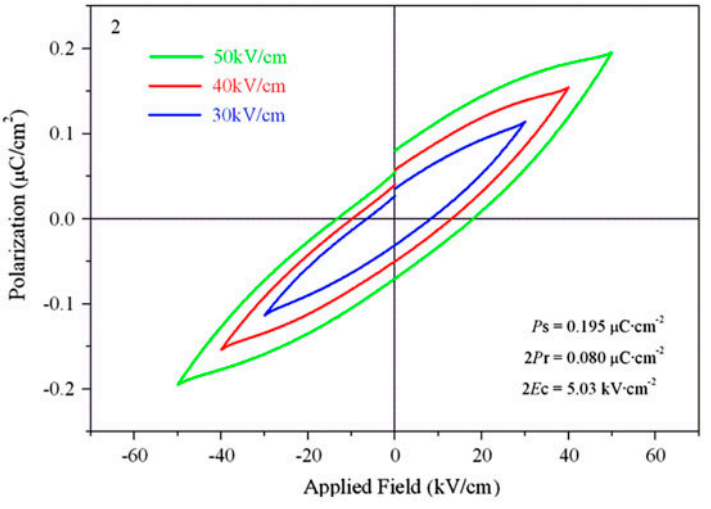

Figure 7. Electric hysteresis loops for a pelletized powdered sample of **2**.

4. Conclusion

Two Cu(II) *m*-hydroxybenzoato complexes, {[Cu(bpy)L](μ2−Cl)(μ2−L)[Cu(bpy)L]}·1.2H2O (**1**) and {[Cu(phen)Cl](μ2−Cl)(μ2−L)[Cu(phen)L]} (**2**), resulted from the reaction of $CuCl_2$, *m*-hydroxybenzoic acid (HL), and NaOH with 2,2'-bipyridine (bpy) or 1,10-phenanthroline (phen) in aqueous methanolic solution at room temperature. Both complexes are characterized by chloro- and carboxylato-bridged dinuclear [Cu(μ2−Cl)(μ2−COO)Cu] cores, in which significant antiferromagnetic interactions ($J = -15.9, -12.2$ cm^{-1}) between Cu^{2+} ions are predominate. There are many paddle-wheel-shaped binuclear copper(II) and other copper clusters reported in literature [36–38], but chloro- and carboxylato-bridged dicopper clusters have never been reported. A search of the CSD also showed no examples of chloro- and carboxylate-bridged dinuclear metal complexes for Co, Ni, Zn, Ag, and Mn. The dimers in **1** are pairwise aggregated to form H-bonded tetranuclear motifs. The acentric, polar **2** represents the first example of a ferroelectric metal *m*-hydroxybenzoate complex. Exploration of hydroxybenzoate-based molecular materials and rational syntheses of MOFs using the dinuclear [Cu(μ2−Cl)(μ2−COO)Cu] cores as secondary building units are underway in our lab.

Supplementary material

Electronic supplementary information available: experimental and simulated PXRD patterns of **1** and **2**; IR spectra of **1** and **2**; thermogravimetric analysis of **1** and **2**. CCDC reference numbers 930036–930037. Supplemental data for this article can be accessed http://dx.doi.org/10.1080/00958972.2013.853053.

Acknowledgments

This project was sponsored by K.C. Wong Magna Fund in Ningbo University and supported by the Scientific Research Fund of Zhejiang Provincial Education Department.

References

[1] J.P. Johnpeter, F. Schmitt, E. Denoyelle-Di-Muro, G. Wagnières, L. Juillerat-Jeanneret, B. Therrien. *Inorg. Chim. Acta*, **393**, 246 (2012).
[2] S.C. Manna, S. Mistri, A.D. Jana. *CrystEngComm*., **14**, 7415 (2012).
[3] R. Biswas, S. Mukherjee, P. Kar, A. Ghosh. *Inorg. Chem.*, **51**, 8150 (2012).
[4] F. Semerci, O.Z. Yeşilel, S. Keskin, C. Darcan, M. Taş, H. Dal. *CrystEngComm*., **15**, 1244 (2013).
[5] L. Li, H. Xu, X.J. Shi, H.W. Hou, Y.T. Fan. *Inorg. Chim. Acta*, **363**, 3939 (2010).
[6] Z.D. Wang, D.R. Powell, R.P. Houser. *Inorg. Chem. Commun.*, **12**, 511 (2009).
[7] S. Mukherjee, P.S. Mukherjee. *Dalton Trans.*, 4019 (2013).
[8] S. Youngme, W. Somjitsripunya, K. Chinnakali, S. Chantrapromma, H. Fun. *Polyhedron*, **18**, 857 (1999).
[9] D. Sadhukhan, A. Ray, R.J. Butcher, C.J. Gomez García, B. Dede, S. Mitra. *Inorg. Chim. Acta*, **376**, 245 (2011).
[10] S.P. Perlepes, J.C. Huffman, G. Christou. *Polyhedron*, **10**, 2301 (1991).
[11] J.-R. Su, D.-J. Xu. *J. Coord. Chem.*, **58**, 629 (2005).
[12] Y. Koizumi, H. Sawase, Y. Suzuki, M. Shimoi, A. Ouchi. *Bull. Chem. Soc. Jpn.*, **57**, 1677 (1984).
[13] A.E. Koziol, W. Brzyska, B. Kltmek, A. Kula, G.J. Palenik, K. Stepniak. *J. Coord. Chem.*, **21**, 183 (1990).
[14] K. Kanamori, K. Yamamoto, K. Okamoto. *Chem. Lett.*, **22**, 1253 (1993).
[15] S. Youngme, A. Cheansirisomboon, C. Danvirutai, C. Pakawatchai, N. Chaichit, C. Engkagul, G.A.V. Albada, J.S. Costa, J. Reedijk. *Polyhedron*, **27**, 1875 (2008).
[16] Y.Q. Zheng, J. Zhang, J.Y. Liu. *CrystEngComm*., **12**, 2740 (2010).
[17] J.H. Kim, J. Baek, P.S. Halasyamani. *Chem. Mater.*, **19**, 5637 (2007).
[18] X.M. Jiang, M.J. Zhang, H.Y. Zeng, G.C. Guo, J.S. Huang. *J. Am. Soc. Chem.*, **133**, 3410 (2011).
[19] Y. Hasegawa, R. Hieda, K. Miyata, T. Nakagawa, T. Kawai. *Eur. J. Inorg. Chem.*, **32**, 4978 (2011).
[20] D.A. Conlon, N. Yasuda. *Adv. Synth. Catal.*, **1**, 343 (2001).
[21] Z.G. Guo, R. Cao, X. Wang, H.F. Li, W.B. Yuan, G.J. Wang, H.H. Wu, J. Li. *J. Am. Chem. Soc.*, **131**, 6894 (2009).
[22] X. Tan, Y.X. Che, J.M. Zheng. *Inorg. Chem. Commun.*, **22**, 10 (2012).
[23] G.A. Bain, J.F. Berry. *J. Chem. Edu.*, **85**, 532 (2008).
[24] G.M. Sheldrick. *SHELXS-97, Program for Crystal Structure Solution*, University of Göttingen, Germany, Göttingen (1997).
[25] G.M. Sheldrick. *SHELXL-97, Program for Crystal Structure Refinement*, University of Göttingen, Germany, Göttingen (1997).
[26] S.K. Dey, B. Bag, K.M.A. Malik, M.S.E. Fallah, J. Ribas, S. Mitra. *Inorg. Chem.*, **42**, 4029 (2003).
[27] A.W. Addison, N. Rao. *J. Chem. Soc., Dalton Trans.*, 1349 (1984).
[28] H.L. Zhu, J.L. Lin, W. Xu, J. Zhang, Y.Q. Zheng. *J. Coord. Chem.*, **64**, 2088 (2011).
[29] I. Persson, P. Persson, M. Sandström, A.-S. Ullström. *J. Chem. Soc., Dalton Trans.*, 1256 (2002).
[30] K.N. Lazarou, I. Chadjistamatis, A. Terzis, S.P. Perlepes, C.P. Raptopoulou. *Polyhedron*, **29**, 833 (2010).
[31] S. Youngme, J. Phatchimkun, N. Wannarit, N. Chaichit, S. Meejoo, G.A.V. Albada, J. Reedijk. *Polyhedron*, **27**, 304 (2008).
[32] S. Youngme, C. Chailuecha, G.A.V. Albada, C. Pakawatchai, N. Chaichit, J. Reedijk. *Inorg. Chim. Acta*, **358**, 1068 (2005).
[33] K. Nakamoto. *Infrared and Raman Spectra of Inorganic and Coordination Compounds*, 4th Edn, Interscience-Wiley, New York (1986).
[34] G.C. Campbell, J.F. Haw. *Inorg. Chem.*, **27**, 3706 (1988).
[35] V.V. Atuchin, B.I. Kidyarov, N.V. Pervukhina. *J. Cryst. Growth*, **275**, e1941 (2005).
[36] Y.M. Li, C.Y. Xiao, H.R. Feng, S.S. Guo, S.B. Wang. *J. Coord. Chem.*, **64**, 1165 (2011).
[37] E.M. Rustoy, M. Agotegaray, O.E. Piro, E.E. Castellano. *J. Coord. Chem.*, **65**, 2341 (2012).
[38] P.M. Selvakumar, S. Nadella, J. Sahoo, E. Suresh, P.S. Subramanian. *J. Coord. Chem.*, **66**, 287 (2013).